Light propagation analysis in nervous tissue for wireless optogenetic nanonetworks

Stefanus Wirdatmadja, Pedram Johari, Sasitharan Balasubramaniam, Yongho Bae, Michal K. Stachowiak, et al.

Stefanus Wirdatmadja, Pedram Johari, Sasitharan Balasubramaniam, Yongho Bae, Michal K. Stachowiak, Josep M. Jornet, "Light propagation analysis in nervous tissue for wireless optogenetic nanonetworks," Proc. SPIE 10482, Optogenetics and Optical Manipulation 2018, 104820R (14 February 2018); doi: 10.1117/12.2288786

SPIE.

Event: SPIE BiOS, 2018, San Francisco, California, United States

Light Propagation Analysis in Nervous Tissue for Wireless Optogenetic Nanonetworks

Stefanus Wirdatmadja[a], Pedram Johari[b], Sasitharan Balasubramaniam[a], Yongho Bae[b], Michal K. Stachowiak[b], and Josep M. Jornet[b]

[a]Tampere University of Technology, Korkeakoulunkatu 10, Tampere, Finland
[b]University at Buffalo, The State University of New York, Buffalo, New York, USA

ABSTRACT

In recent years, numerous methods have been sought for developing novel solutions to counter neurodegenerative diseases. An objective that is being investigated by researchers is to develop cortical implants that are able to wirelessly stimulate neurons at the single cell level. This is a major development compared to current solutions that use electrodes, which are only able to target a population of neurons, or optogenetics, which requires optical fiber-leads to be embedded deep into the brain. In this direction, the concept of wireless optogenetic nanonetworks has been recently introduced. In such architecture, miniature devices are implanted in the cortex for neuronal stimulation through optogenetics. One of the aspects that will determine the topology and performance of wireless optogenetic nanonetworks is related to light propagation in genetically-engineered neurons. In this paper, a channel model that captures the peculiarities of light propagation in neurons is developed. First, the light propagation behavior using the modified Beer-Lambert law is analyzed based on the photon transport through the nervous tissue. This includes analyzing the scattering light diffraction and diffusive reflection that results from the absorption of neural cell chromophores, as well as validating the results by means of extensive multiphysics simulations. Then, analysis is conducted on the path loss through cells at different layers of the cortex by taking into account the multi-path phenomenon. Results show that there is a light focusing effect in the soma of neurons that can potentially help the to stimulate the target cells.

Keywords: Optogenetics, Single-neuron Stimulation, Light Propagation, Wireless Nanonetworks

1. INTRODUCTION

In recent years the field of Brain Machine Interfaces (BMI) has led to numerous research initiatives aimed at developing new solutions to interfacing to neural systems. These initiatives are discovering new solutions ranging from neuron stimulation for patients who suffer from neurodegenerative diseases, all the way to the most recent vision of interfacing the brain to computing systems to enhance their capabilities.

A traditional approach for stimulating the brain is through the use of electrodes. However, a major limitation is the large population of neurons that get targeted during stimulation. This has led the research community to develop new approaches to stimulate at single-cell level. The field of optogenetics enables single cells to be stimulated using light at a specific wavelength. This requires that neurons are first engineered with genes that will express proteins to make the neurons sensitive to light, where the emission of the lights can both activate or inhibit the neuron's action potential. Since the original proposed optogenetics architecture, which requires an insertion of optical cable into the skull, wireless device models have also been proposed to provide more autonomy in the subjects that require stimulation.[1,2,3] Most recently, we proposed integrating the concept of wireless optogenetic for devices constructed from nanoscale components, i.e., Wireless Optogenetic Nanonetworking Device (WiOptND), where these devices could form nanonetworks to coordinate stimulations.[4]

Further author information: (Send correspondence to Pedram Johari)
Stefanus Wirdatmadja: E-mail: stefanus.wirdatmadja@tut.fi
Pedram Johari: E-mail: pedramjo@buffalo.edu, Telephone: 1 (716) 907-3086
Sasitharan Balasubramaniam: E-mail: sasib@tssg.org
Yongho Bae: E-mail: yonghoba@buffalo.edu
Michal K. Stachowiak: E-mail: mks4@buffalo.edu
Josep M. Jornet: E-mail: jmjornet@buffalo.edu

Optogenetics and Optical Manipulation 2018, edited by Samarendra K. Mohanty, Nitish V. Thakor, E. Duco Jansen,
Proc. of SPIE Vol. 10482, 104820R · © 2018 SPIE · CCC code: 1605-7422/18/$18 · doi: 10.1117/12.2288786

An important element in the wireless optogenetics is the light stimulation process between the device and the target neurons. New constraints will need to be considered compared to previous approaches, and in particular due to the nanoscale components of the light source as well as energy produced by the device. Since the light component is miniaturized, this means that its location within the neuron population and distance from the target cell are important factors to understand the required intensity for stimulating the neuron. The location within the neural population, as well as its density and connectivity is an important factor, since the light reflection and scattering from the neighboring cells will affect the intensity at the target cell.[5,6] This also varies within the cell population, since certain regions will have sparse density of somas that are largely filled with axons and dendrites, while in other regions dense somas will be found. Each of these cases will affect the light intensity that arrives at the target cell. Indirectly, this will also be impacted by the distance between the light source to the target cell.

In this paper, we develop a channel model for wireless optogenetic nano communication. The nano spacing considered for the channel model is between the light source and the target neuron. We develop geometric analysis to consider the light propagation, reflection, refraction, as well as scattering from the neighboring cells and how this impacts on the intensity at the target cells. Our channel model also considers the variation that is due to the density of neighboring somas and dendrites, as well as the shapes and structures of the cells. In a nutshell, by understanding the behavior of light in the brain tissues, efficient design for BMI can be achieved and the implants are feasible for long term operation and wirelessly interact with neurons forming the reliable optogenetic nanonetworks.

The remainder of the paper is organized as follows. In Section 2 we will define a system model including architecture for wireless optogenetic nanonetworking and the fundamental of light propagation in biological tissues. Section 3 contains a complete light propagation channel model for a single cell as well as the numerical analysis and results.In Section 4, we consider the multipath scenario due to the heterogeneous neuron population. Finally, we conclude the paper in Section 5.

2. SYSTEM MODEL

2.1 Wireless Optogenetic Nanonetwork Architecture

The entire network of the Wireless Optogenetic Nanonetworking architecture is composed of three layers (Figure 1). The lowest layer is the cerebral cortex where WiOptNDs are deployed and interfaced to individual neurons that require stimulation (Figure 2). The cerebral cortex is the gray matter of the brain and is responsible for sensory, motor, and associated functions. Horizontally, the cerebral cortex is categorized based on its functional areas, namely, the molecular layer, the external granular layer, the external pyramidal layer, the internal granular layer, the internal pyramidal layer, and the multiform layer. Those layers contain various types of cells, including pyramidal cells, spiny stellate cells, basket cells, chandelier cells, and smooth stellate cells,[7] each of which can have an interfaced WiOptND. The next layer up is the sub-dura transceiver, which is located on the dura and below the skull, and communicates with the WiOptNDs. The role of the sub-dura transceiver is to emit ultrasound waves, which are used to charge the WiOptND. The sub-dura transceiver contains the algorithm that determines both the charging and stimulation sequence of the WiOptND, and this in turn emits the sequence of ultrasound signals. Above the sub-dura transceiver is the external transceiver, which communicates with the sub-dura transceiver. While the communication between the external transceiver and the sub dura transceiver is a very relevant aspect of the system, our focus is on the interfacing of the individual WiOptNDs with neurons through light.

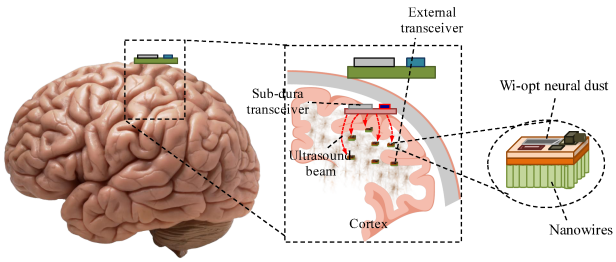

Figure 1: Illustration of the overall architecture of the Wireless Optogenetic Nanonetwork. The WiOptND are scattered in the various layers of the cortex, and is charged by the ultrasound signals emitted from the *sub-dura transceiver*, which in turn is communicated from the *external transceiver*.

Figure 2: Illustration of a WiOptND that interfaces to an engineered neuron that is sensitive to light at a specific wavelength.

2.2 Fundamentals of Light Propagation in Biological Tissues

When the light propagates in the biological tissue, there are four main phenomena that might occur (Figure 3).

- *Scattering*, which can be perceived as deflection of the ray of light from a straight path due to heterogeneous medium or the interface between two media. As the light experiences scattering, it might be transmitted or back scattered. Light scattering in biological tissues is well defined by the *Henyey-Greenstein* phase function introducing the coefficient *anisotropy factor, g*.[8] For biological tissues, typically this parameter is in the range of $0.5 \leq g \leq 0.95$, which indicates that forward scattering is dominant.[8] For a more accurate model of light propagation in biological tissues, the reduced scattering parameter, $\mu_s' = (1-g)\mu_s$, is used since the light undergoes multiple scattering effect.[8]
- *Absorption*, where the light energy is absorbed and converted to heat as the result of atoms and molecule vibration. The atoms and molecules have the selective natural behavior of certain light frequency absorption. For wavelength used in optogenetics, which is less than 625 nm, the absorption parameters are in the range of $0.5 - 5$ cm^{-1}.[8]

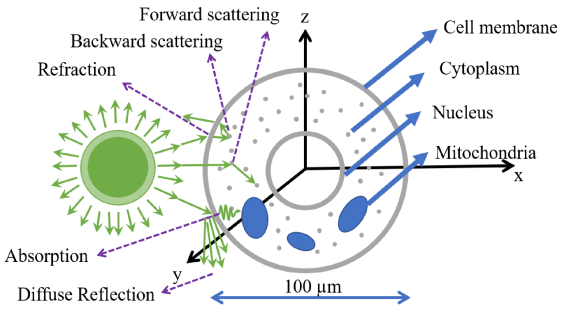

Figure 3: Model of refraction, reflection, absorption, and scattering of light on a neuron's soma.

- *Reflection* is the phenomenon where the the direction of the light propagation is reflected back to the same medium as it is originated. For biological tissues, diffuse reflection is most likely to occur. The common simplification for biological environment is by assuming that the surface is *Lambertian*.[9]
- *Refraction* occurs due to the light traversing via two media with different density. This causes the change in propagation direction. This phenomenon is described by *Snell's law* where ratio of the angle of incident θ_i and refraction θ_r is proportional to the phase velocities (v_1/v_2), or equivalently, inversely proportional to refraction indices of the two media (n_2/n_1):

$$\frac{sin\theta_i}{sin\theta_r} = \frac{v_i}{v_r} = \frac{n_r}{n_i}. \tag{1}$$

3. SINGLE CELL CHANNEL MODEL

3.1 Analytical Model

The light transportation through biological tissue can be modeled using the modified Beer-Lambert law as:

$$I(\lambda) = I_0(\lambda)e^{-\mu_a(\lambda)dDPF(\lambda)+G(\lambda)}, \tag{2}$$

where $I(\lambda)$ is the measured λ wavelength light intensity on distance d, $I_o(\lambda)$ is the light intensity on the source, μ_a is the absorption coefficient of the biological tissue, $DPF(\lambda)$ is the differential path length, which indicates the mean light propagation distance in the tissue, and $G(\lambda)$ is a wavelength, medium, and geometry dependent constant. The value of the DPF depends on the medium characteristics including absorption (μ_a) and reduced scattering (μ_s') as follows:[10]

$$DPF(\lambda) = \frac{1}{2}\left(\frac{3\mu_s'(\lambda)}{\mu_a(\lambda)}\right)^{1/2}\left[1 - \frac{1}{1+d(3\mu_a(\lambda)\mu_s'(\lambda))^{1/2}}\right]. \tag{3}$$

The distance parameter d is less significant when $d > 2.5$ cm and $d\sqrt{3\mu_a\mu_s'} \gg 1$. Given the very small separation between the WiOptNDs and neurons, this parameter is crucial for DPF calculation.

As mentioned in Section 2.2, the traversing light rays undergo refraction phenomenon. Part of the rays, which are transmitted through the cells, experience the propagation through two different media with different refractive indices. This has been further analyzed in Johari et al.[11] that the transmitted light is focused to certain points on the other side of the illuminated part of the cell. Understanding this phenomenon is important in optogenetics considering the heterogeneous population of neurons in the cortex. The light might penetrate beyond neurons and excite a neuron in a dense neuron population. The most important aspects for optogenetics experiencing this situation is how far the light propagates after traversing through neuron and what is its intensity as illustrated on Figure 4.

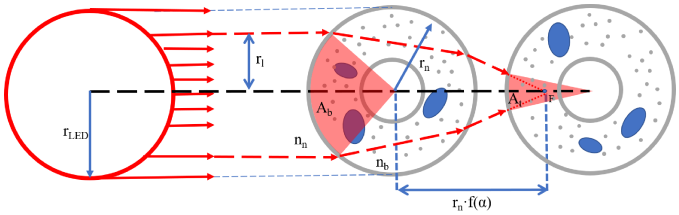

Figure 4: Illustration of light propagation with a light source, a blocking neuron, and a target neuron.

In this first model, for mathematical tractability, we model neurons as spherical cells due to its shape of roughly spherical.[12,13] The distance between the center of a spherical cell and focus point is $r_n f(\alpha)$, where α is the ratio of $\frac{r_l}{r_n}$. The lower and upper bounds, $f_l(\alpha \to 0)$ and $f_u(\alpha \to 1)$ of the focal points are dictated by the real part of refractive indices of the media that the light traverse through as:[11]

$$\begin{aligned} f_l(\alpha) &= \frac{n_n^2}{2n_b\sqrt{n_n^2 - n_b^2}}, \quad \text{when } \alpha \to 0; \\ f_u(\alpha) &= \frac{n_n}{2(n_n - n_b)}, \quad \text{when } \alpha \to 1, \end{aligned} \tag{4}$$

where n_b and n_n are the refractive indices of brain tissue and neuron respectively. The distance of focus points from the center of the neuron is defined as $r f_{l/u}(\alpha)$.

The light propagation decreases the intensity due to scattering and absorption while the focusing effect of the cell aggregates the light rays, which increases the intensity. This focusing effect aggregates the light power with respect to the ratio of spherical caps of both blocking, A_b and target neurons, A_t. The values of A_b and A_t can be obtained by geometrically analyzing the solid angles, β_b and β_t, from the focus point angle ψ as shown in Figure 5. Assuming that the half surface of total spherical cell of blocking neuron is illuminated by the light source, the effective arc, $2\beta_b$, is π rad, while the effective arc of the target neuron depends on the focus point and it can be formulated as:

$$2\beta_t = 2\psi\frac{r_n f(\alpha) - d_{ss} - r_n}{r_n}. \tag{5}$$

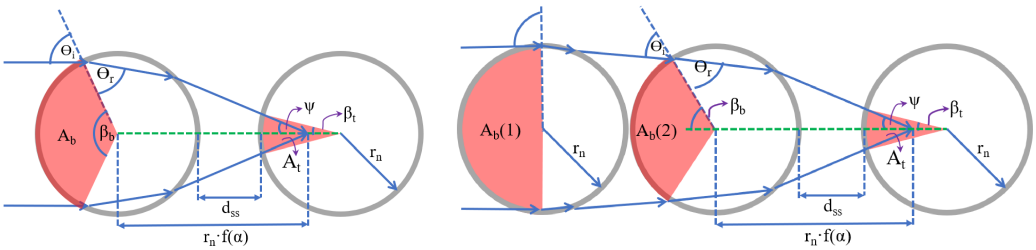

(a) One blocking neuron and a target neuron. (b) Two blocking neurons and a target neuron.

Figure 5: Refraction and focusing effect due to blocking neuron(s).

Note that the maximum value of the intensity is achieved when $rf_u(\alpha) = r_n + d_{ss}$, which means the light rays focus at a single point on the target neuron surface. The solid angles and spherical cap of both blocking and target neurons can be obtained by:

$$\omega_{b/t} = 2\pi(1 - cos\beta_{b/t}), \tag{6}$$

$$A_{b/t} = \omega_{b/t} r_n^2, \tag{7}$$

where subscript b/t indicates either blocking or target neuron.

The final intensity after the blocking neuron penetration depends on the light-exposed spherical cap area ratio γ between the blocking neuron A_b and the target neuron A_t. Thus, the final intensity can be formulated as:

$$\begin{aligned} I_t &= \frac{A_b}{A_t} I_o e^{-\mu_a^i(\lambda) d_i DPF_i + G(\lambda)} \\ &= \gamma\, I_o e^{-\mu_a^i(\lambda) d_i DPF_i + G(\lambda)}. \end{aligned} \tag{8}$$

For multiple blocking neurons between light source and target neuron, the focus distance should be calculated based on the output of the previous blocking neuron. Therefore, the distance of focus point can be obtained by:[11]

$$r_n f(\alpha) = r_n \frac{sin(\pi - \theta_i)}{sin(\theta_i - \theta_r)}. \tag{9}$$

3.2 Numerical Results

Table. 1 lists the parameters used in the MATLAB simulation. Figure 6 shows the output intensity, path loss, and time delay characteristics comparison among three difference cases. For the output intensity, *no-blocking* case shows no significant changes, while cases with blocking neuron, intensity tends to rise and followed by decrements due to focusing effect of the light rays. Maximum intensity reaches when the rays focus to approximately infinitesimal point. This effect can be explained theoretically by ratio γ in (8) with the target neuron spherical area A_t as the denominator. Not only γ, the focus point $rf(\alpha)$ determines at which distance the maximum intensity occurs. Without blocking neuron(s), the propagation path loss tends to decrease faster since the energy propagate to all directions, unlike in the presence of blocking neurons where the light energy aggregates due to the effect of the blocking cell. Regarding the light ray arrival to the target neuron, the blocking neurons causes more propagation delay. This mainly depends on the light speed on the medium, which depends on refractive index. In this simulation, the speed of light propagating via neuron is 2.05×10^8 m/s, while via brain tissue, the speed is 2.15×10^8 m/s. Therefore, the more blocking neurons between light source and target neuron, the delay increases. However, the delay is considered small and the whole transmission process is only within pico second unit (one blocking neuron introduces additional delay of approximately 0.02 pico seconds).

To further validate the light focusing effect in the neurons, we have run extensive simulations by using COMSOL Multiphysics.[18] Photon diffusion by solving *Helmholtz Equations* has been considered to simulate the light propagation through the soma of neurons as shown in Figure 7. This figure shows the propagation of light through the nervous tissues when (a) there is no neuron and (b) there are three neurons in a row. The pattern intensity depicted on Figure. 7 shows the

Table 1: Simulation Parameters

Parameter	Value [Unit]	Description
r_n	50 [μm]	Spherical radius of neuron
$\bar{\rho}$	0.5 [%]	Reflectance index of neuron[14]
v_{vacuum}	3×10^8 [m/s]	Speed of light in vacuum
λ	456 [nm]	Wavelength of light
n_b	1.35	Refractive index of brain tissue[15]
n_n	1.36	Refractive index of neuron
$\phi_{1/2}$	$\frac{55}{180}$ [rad]	Half power point angle
$\mu_{a_{neuron}}$	0.9 [/mm]	Absorption coefficient of neuron[16]
$\mu'_{s_{neuron}}$	3.43 [/mm]	Reduced scattering coefficient of neuron[16]
$\mu_{a_{tissue}}$	20 [/mm]	Absorption coefficient of brain tissue[17]
$\mu'_{s_{tissue}}$	1.34 [/mm]	Reduced scattering coefficient of brain tissue[17]

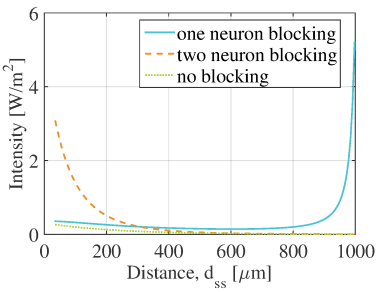

(a) Light intensity.

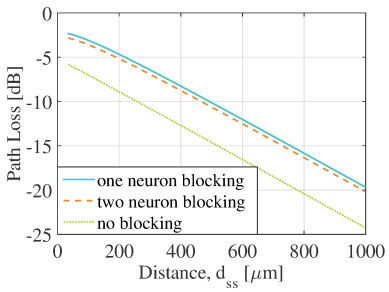

(b) Path Loss.

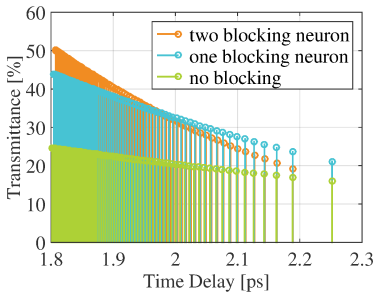

(c) Time Delay of rays of light arriving the surface of target neuron after two blocking neurons.

Figure 6: Light measurements on the surface of the target neurons. The distance between blocking and target neuron (d_{ss}) is varied for (a) and (b), while it is kept constant on (c).

possibility of farther extension where neurons are positioned along the propagation path. The color map indicates the soma has positive effect in increasing the light propagation distance due to focusing effect phenomenon. Therefore, the blocking neuron scenario can be exploited in the dense neuron population environment.

Figure 8 shows the photon counts in a logarithmic scale to compare the *with-* and *without-neuron* scenarios. Measuring the perpendicular path from the source, the *with-neuron* scenario is able to maintain the light intensity longer. At around the distance of 400μm from the light source, the intensity difference between two scenarios is approximately 18 dB. Each neuron along the propagation path contributes in maintaining the higher intensity longer with respect to distance. Considering the neuron diameter of 100μm, the intensity is approximately 6 dB higher after the light traverses the neuron.

4. MULTIPATH PROPAGATION MODEL

Considering the heterogeneous neuron population in the brain tissue, the light propagation in the tissue might include three components, namely, a line of sight (LoS) component, time delayed components, and reflected components.

4.1 Analytical Model

In this case, the power delay profile (PDP) can be used to analyze the light intensity with regards to multipath channel as a function of time delay. The PDP for LoS component is given by:[19]

$$h^{(0)}(t;\Phi_0) = L_0 P_0 \delta\left(t - \frac{d_0}{c}\right), \tag{10}$$

where

$$L_0 = e^{-\mu_a(\lambda) d_0 DPF(\lambda) + G(\lambda)}. \tag{11}$$

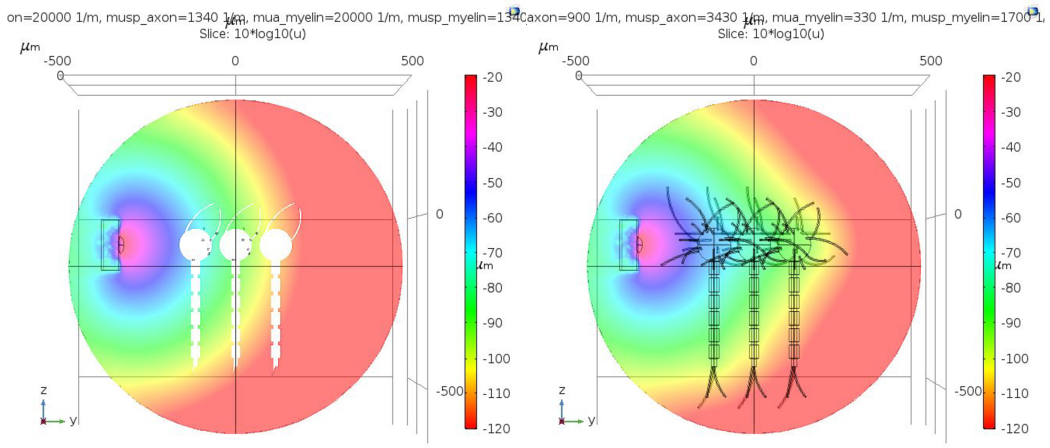

Figure 7: COMSOL simulations for light propagation in nervous tissue a) without neurons b) with three neurons.

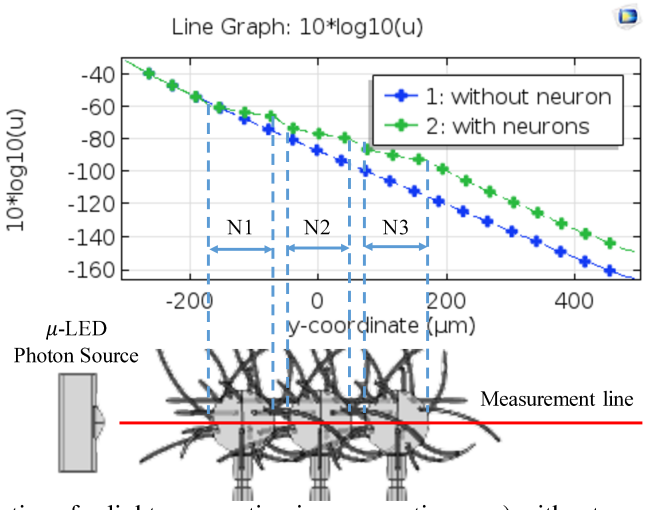

Figure 8: COMSOL simulations for light propagation in nervous tissues a) without neurons b) with three neurons.

For the reflected component (after k bounces), the PDP is given by:

$$h^k(t;\Phi) = \int_S \left[L_1 L_2 ... L_{k+1} \Gamma^{(k)} \times \delta\left(t - \frac{d_1 + d_2 + ... d_{k+1}}{c} \right) \right] dA_{ref}, k \geq 1, \tag{12}$$

where each path-loss term for each paths is represented by:

$$L_1 = \frac{A_{ref}^1}{2\pi d_1^2} e^{-\mu_a(\lambda) d_1 DPF(\lambda) + G(\lambda)} \iint (m+1) cos^m \phi_1 \, cos\theta_1 \, d\phi_1 \, d\theta_1,$$

$$L_2 = \frac{A_{ref}^2}{2\pi d_2^2} e^{-\mu_a(\lambda) d_2 DPF(\lambda) + G(\lambda)} \iint cos\phi_2 \, cos\theta_2 \, d\phi_2 \, d\theta_2, ...,$$

$$L_{(k+1)} = \frac{A_{eff}^{target}}{2\pi d_{(k+1)}^2} e^{-\mu_a(\lambda) d_{(k+1)}^2 DPF(\lambda) + G(\lambda)} \iint cos\phi_{(k+1)} \, cos\theta_{(k+1)} \, d\phi_{(k+1)} \, d\theta_{(k+1)}.$$

The PDP is integrated with respect to all neighboring neuron S and A_{ref} is the effective area on which the light is reflected.The directivity of the light source can be represented as $m = -1/log_2(cos\phi_{1/2})$, where $2\phi_{1/2}$ indicates the angle

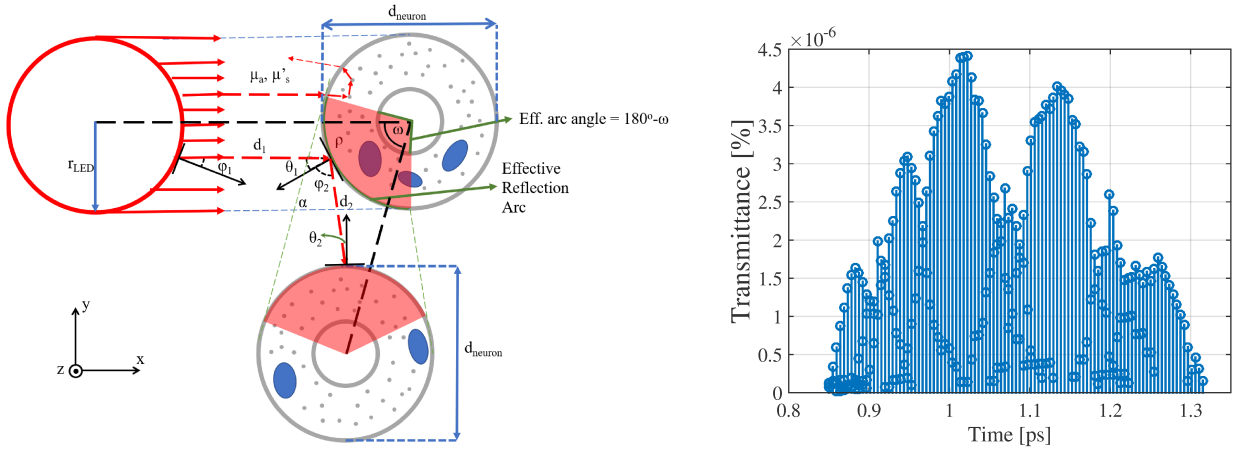

(a) One blocking neuron and a target neuron.

(b) Two blocking neurons and a target neuron.

Figure 9: One hop reflection model.

of the light half power point. The angles of irradiance and incidence are represented by ϕ_k and θ_k respectively. The speed of light in the brain tissue is represented by c. The parameter d_k is the distance between light source and target neuron.

The reflected power after k bounces is represented by:

$$\Gamma^{(k)} = P_0\bar{\rho}_1\bar{\rho}_2...\bar{\rho}_k = k\,\bar{\rho}\,P_0 = k\left[\frac{n_b - n_n}{n_b + n_n}\right]^2 P_0, \tag{13}$$

where $\bar{\rho}$ is the reflectance index.

Finally the total PDP can be obtained by:

$$h(t) = \sum_{k=0}^{N_{adj}} h^k(t;\Phi_n). \tag{14}$$

Figure 9(a) illustrates two dimensional projection of one hop light reflection. The LoS component is not illustrated and the light rays are propagated on the x-axis and polarized on the y-axis. The A_{ref} is obtained by intersecting the projected area of the LED and the target neuron to the reflecting neuron. When $\angle\omega$ represents the angle connecting the center of the LED, reflecting neuron, and target neuron, the effective reflection arc angle is $\angle(180^o - \omega) = (\pi - \omega)$ rad. Let the azimuthal and polar angle of the cone formed between the center and the surface of the neuron be ω' and β respectively, the solid angle Ω can be calculated by:

$$\Omega = \iint_S \sin\omega'\,d\alpha'\,d\beta = \int_0^{2\pi}\int_0^{\frac{1}{2}(\pi-\omega)} \sin\omega'\,d\omega'\,d\beta = 2\pi(1-\sin\frac{1}{2}\omega). \tag{15}$$

Thus, the spherical cap of the cone, which represents the reflecting area A_{ref}, can be obtained by:

$$A_{ref} = \Omega r_{neuron}^2. \tag{16}$$

4.2 Numerical Results

The time delay caused by the path of the light propagation hitting the *Lambertian* surface is shown in Figure 9(b). The power transmittance of reflection components is very low since the reflectance index of neuron cell is very low ($\approx 0.5\%$[14]) and the multipath time is approximately 0.5 pico seconds for one reflecting neuron.

The in-vivo neuron population structure is randomly scattered, therefore, the reflection interference might occur due to this reason. Figure 10(a) depicts one case where *Light source 2* unintentionally illuminates cell *Target 1* with the light reflected by cell *Target 2*. The simulation is conducted by varying both the angle ω and the distance d_{ss}. The output shows that the pathloss is so high (more than 80 dB) that the light interference does not cause any significant effect to the undesired target (Figure 10(b)).

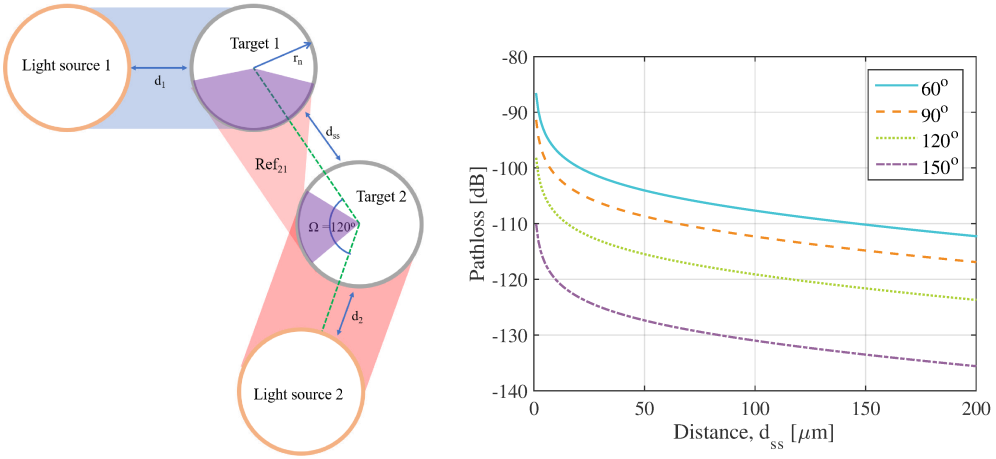

(a) Reflection interference caused by undesired light source from neighboring neuron.

(b) The path loss of the reflection caused by interference of undesired light source from neighboring target neuron as the function of distance.

Figure 10: Reflection intereference model.

5. CONCLUSION

Considering the brain morphology where diverse population of neurons in the neocortex can effect the light propagation for optogenetics at the nanoscale, deeper analysis on the phenomenon is required to observe its behavior at such scale. The interaction of the light wave on the biological tissue includes a combination of scattering, absorption, reflection, and refraction, where all this depends on the optical and geometry properties of the light wave on the medium and the neurons. Taking into consideration the optical properties while assuming spherical geometry of neuron for simplification, the focusing effect occurs as the light wave propagates in the brain tissue. This phenomenon results in an intensity increase ($\approx$ 6 dB/neuron for 100 μm diameter neuron) once the light wave leaves the soma. The analysis is based on the one axis polarized light propagation on the soma that is perfectly aligned to the propagation path. The COMSOL simulation confirms the focusing effect resulting in farther light propagation when the blocking neurons exist between the light source and the target neuron. With respect to the delay, blocking neurons cause insignificant delay (at the pico second level).

At the same time, the effect of reflection is extremely small compared to the LoS component so the interference from adjacent neurons can be ignored. The reason for this is because, for each hop of reflected light rays, the reflected light power is multiplied by a very small value of reflectance coefficient. The reflection analysis has considered the angle of the neurons for various possible position in the brain. Based on the blocking and multipath propagation models, we found that highly dense neuron population can benefit from having a blocking neuron in between a light source and the target neuron, to assist in directing and increasing the light intensity required for successful stimulation.

ACKNOWLEDGMENTS

This work is supported by the Academy of Finland Research Fellow program under project no. 284531. This work has also been supported by the European Union Horizon 2020 CIRCLE project under the grant agreement No. 665564. This publication has also emanated from research supported in part by the Science Foundation Ireland (SFI) CONNECT research centre, which is co-funded under the European Regional Development Fund under Grant Number 13/RC/2077. This work was also supported by the U.S. National Science Foundation (NSF) under Grants No. CBET-1555720 and CBET-1706050.

REFERENCES

[1] Lee, J. H., Durand, R., Gradinaru, V., Zhang, F., Goshen, I., Kim, D.-S., Fenno, L. E., Ramakrishnan, C., and Deisseroth, K., "Global and local fmri signals driven by neurons defined optogenetically by type and wiring," *Nature* **465**(7299), 788 (2010).

[2] Liu, X., Ramirez, S., Pang, P. T., Puryear, C. B., Govindarajan, A., Deisseroth, K., and Tonegawa, S., "Optogenetic stimulation of a hippocampal engram activates fear memory recall," *Nature* **484**(7394), 381–385 (2012).

[3] Chaudhury, D., Walsh, J. J., Friedman, A. K., Juarez, B., Ku, S. M., Koo, J. W., Ferguson, D., Tsai, H.-C., Pomeranz, L., Christoffel, D. J., et al., "Rapid regulation of depression-related behaviors by control of midbrain dopamine neurons," *Nature* **493**(7433), 532 (2013).

[4] Wirdatmadja, S. A., Balasubramaniam, S., Koucheryavy, Y., and Jornet, J. M., "Wireless optogenetic neural dust for deep brain stimulation," in [*e-Health Networking, Applications and Services (Healthcom), 2016 IEEE 18th International Conference on*], 1–6, IEEE (2016).

[5] Johari, P. and Jornet, J. M., "Nanoscale optical wireless channel model for intra-body communications: Geometrical, time, and frequency domain analyses," *IEEE Transactions on Communications* (2018).

[6] Guo, H., Johari, P., Jornet, J. M., and Sun, Z., "Intra-body optical channel modeling for in vivo wireless nanosensor networks," *IEEE Transactions on NanoBioscience* **15**(1), 41–52 (2016).

[7] Mountcastle, V. B., [*Perceptual neuroscience: the cerebral cortex*], Harvard University Press (1998).

[8] Klose, A. D. and Larsen, E. W., "Light transport in biological tissue based on the simplified spherical harmonics equations," *Journal of Computational Physics* **220**(1), 441–470 (2006).

[9] Xia, J. and Yao, G., "Angular distribution of diffuse reflectance in biological tissue," *Applied optics* **46**(26), 6552–6560 (2007).

[10] Scholkmann, F. and Wolf, M., "General equation for the differential pathlength factor of the frontal human head depending on wavelength and age," *Journal of Biomedical Optics* **18**(10), 105004–105004 (2013).

[11] Johari, P. and Jornet, J. M., "Nanoscale optical channel modeling for in vivo wireless nanosensor networks: A geometrical approach," *Proc. of the IEEE International Conference on Communications (ICC)* , 1–6 (2017).

[12] Andrew, A. M., "Spiking neuron models: Single neurons, populations, plasticity," *Kybernetes* **32**(7/8) (2003).

[13] Quan, T., Zheng, T., Yang, Z., Ding, W., Li, S., Li, J., Zhou, H., Luo, Q., Gong, H., and Zeng, S., "Neurogps: automated localization of neurons for brain circuits using l1 minimization model," *Scientific reports* **3** (2013).

[14] Fang-Yen, C. and Feld, M. S., "Intrinsic optical signals in neural tissues: measurements, mechanisms, and applications," 219–235, ACS Publications (2007).

[15] Levinson, A. and Serby, A., "The refractometric and viscosimetric indexes of cerebrospinal fluid," *Archives of Internal Medicine* **37**(1), 144–150 (1926).

[16] Yaroslavsky, A., Schulze, P., Yaroslavsky, I., Schober, R., Ulrich, F., and Schwarzmaier, H., "Optical properties of selected native and coagulated human brain tissues in vitro in the visible and near infrared spectral range," *Physics in Medicine and Biology* **47**(12), 2059 (2002).

[17] Bosschaart, N., Edelman, G. J., Aalders, M. C., van Leeuwen, T. G., and Faber, D. J., "A literature review and novel theoretical approach on the optical properties of whole blood," *Lasers in medical science* **29**(2), 453–479 (2014).

[18] [*COMSOL Multiphysics Simulation Software*], COMSOL. [Online]. Available: http://www.comsol.com/products/multiphysics/.

[19] Lee, K., Park, H., and Barry, J. R., "Indoor channel characteristics for visible light communications," *IEEE Communications Letters* **15**(2), 217–219 (2011).